Multimodal Freezing System for Cryogenic 3D Printing

Pushkar Prakash Kamble (pushkarkamble@gmail.com)
Indian Institute of Technology Bombay https://orcid.org/0000-0001-8161-4255
Subodh Chavan
Indian Institute of Technology Bombay
Rajendra Hodgir
Indian Institute of Technology Bombay
Gopal Gote
Indian Institute of Technology Bombay
K P Karunakaran
Indian Institute of Technology Bombay
Sandeep Goli
Indian Institute of Technology Bombay

Research Article

Keywords: Cryogenic 3D printing, Multimodal freezing system, Vapor Compression Refrigeration, Additive Manufacturing, Cooling Technology

Posted Date: May 3rd, 2021

DOI: https://doi.org/10.21203/rs.3.rs-480124/v1

Multimodal Freezing System for Cryogenic 3D Printing

*Pushkar Kamble, Subodh Chavan, Rajendra Hodgir, Gopal Gote, K P Karunakaran, Sandeep Goli

Indian Institute of Technology Bombay, Powai, Mumbai-400076, India.

*Corresponding Author Email: pushkarkamble@gmail.com

Abstract:

Cryogenic 3D Printing (Cryo-3DP) creates 3D objects by deposition-then-freezing of aqueous solutions of various materials layer-by-layer. The process generally takes place at the temperature ranging from -20 °C to -25°C. At the beginning of the process, cryo-3DP demands a high cooling rate to reduce the work envelope's temperature rapidly. After the work envelope reaches the working temperature (-20 to -25°C), lower cooling rates are enough. The proposed multimodal freezing system uses two modes of cooling. Rapid injection of the CO_2 gas in the chamber is suitable for achieving high cooling rates (0.5 °Cs^{-1}) initially and *Vapor Compression Refrigeration (VCR)* for sustained heat removal from the system (0.5 °$Cmin^{-1}$). The results show that the proposed multimodal system performs faster than the conventional system.

Keywords: Cryogenic 3D printing, Multimodal freezing system, Vapor Compression Refrigeration, Additive Manufacturing, Cooling Technology

Nomenclature:

Abbreviations		*English Alphabets*	
Cryo-3DP	Cryogenic 3D printing	Nu	Nusselt number
Ice-AM	Ice Additive Manufacturing	Re	Reynolds number
PUF	Polyurethane foam	Pr	Prandtl number
VCR	Vapour Compression Refrigeration	Gr	Grashoff's number
RE	Refrigeration effect	h_{coil}	Convective heat transfer coefficient of the refrigeration coils
MFS	Multimodal Freezing System	h_{plate}	Heat transfer coefficient of the plate for VCR system
English alphabets		h_{co2}	Convective heat transfer coefficient for CO_2 system
Q_{Total}	Total cooling loads	h	Enthalpy of refrigerant
Q_A	Cooling load corresponding to the physical parts of the chamber	h_l	Enthalpy of the liquid
Q_B	Cooling load corresponding to the chamber medium	h_{sup}	Enthalpy of the superheated
Q_C	Cooling load corresponding to the water inlet	h_{sv}	Enthalpy of the saturated vapour
Q_D	Cooling load corresponding to the nozzle heater	h_{sl}	Enthalpy of the saturated liquid form of the refrigerant
Q_E	Cooling load corresponding to the air infiltration	A_{plate}	Area of the work platform
$\dot{Q_{CO_2}}$	Heat absorbed by CO_2	A	Area of the orifice
$\dot{Q}_2$	Heat absorbed by the refrigeration coils	A_{coil}	Area of the refrigeration coils
q	Heat produced by the nozzle heater	L	Latent heat of freezing of water
$C_{p_{Al}}$	Isobaric specific heat capacity of aluminium	T_s	Saturation temperature
C_{p_w}	Isobaric specific heat capacity of water	T_{sl}	Saturation temperature of the liquid refrigerant
$C_{p_{air}}$	Isobaric specific heat capacity of the air	T_{sv}	Saturated vapour temperature the refrigerant
$C_{p_{co2}}$	Isobaric specific heat capacity of CO_2	T_l	Temperature of the liquid
m_{wp}	Mass of work platform	P_{up}	Upstream pressure
m_{rod}	Mass of support rods		
$\dot{m}_{choked}$	Mass flow rate of CO_2		
m_{air}	Mass of chamber air	***Greek alphabets***	
$\dot{m_w}$	Mass flow rate of water	ΔT	Temperature drop
ρ	Gas density	ΔP	Pressure drop
W	Compressor work	μ_{JT}	Joule-Thomson's coefficient
C	Dimensionless discharge coefficient	κ	dimensionless ratio of the heat capacities at constant pressure to constant volume

1. Introduction

The process of *Cryogenic 3D Printing (Cryo-3DP)* is carried out at sub-zero temperatures, typically around -20 °C to -25 °C [1-4]. The process starts with the cooling of the work chamber from the room temperature to -20 °C to -25 °C. Once the temperature of the work chamber is achieved, the material deposition subsystem spreads the liquid layer selectively on the work platform. Motion subsystem maneuvers the deposition head as per the required layer geometry. The deposited layer instantly solidifies. Another layer of the liquid is selectively spread on the previous layer, that undergoes freezing. The process continues till many such layers are deposited onto one another, realizing the three-dimensional object [1][5-8].

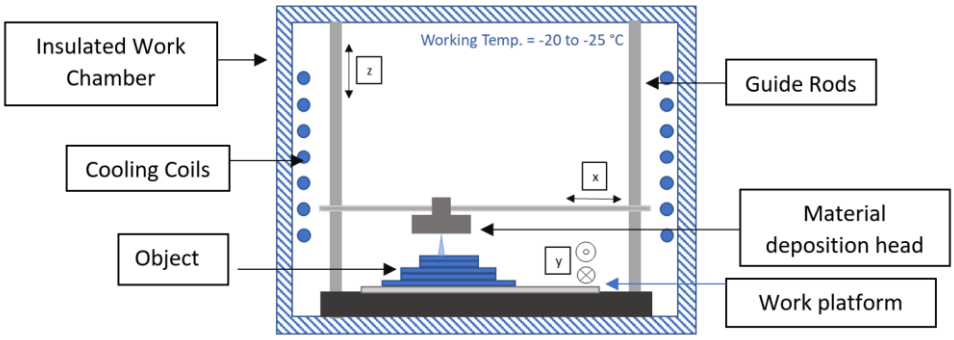

Fig. 1 Schematic Diagram of a Cryogenic 3D Printer

Fig. 1 shows the schematic diagram of the typical cryogenic 3D printer. The deposition and motion systems are enclosed in the work chamber that is insulated to maintain the sub-zero temperatures. The cooling is provided by the refrigeration system.

The process of cryogenic 3D printing finds applications in the field of investment casting (see Fig. 2) [5], photopolymer additive manufacturing for the support structure [7], drug encapsulation in the pharma industry [8-9], micro – manufacturing[10] and architectural models[6].

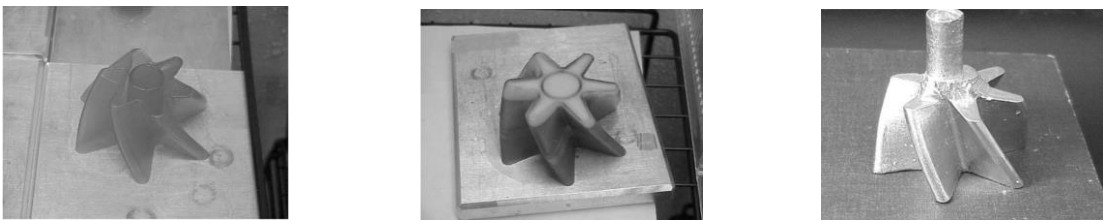

(a) 3D Printed Ice boundary (b) Block of Ice as a Pattern (c) Cast Part

Fig. 2 Cryo-3DP of Ice : Ice as a Pattern for Investment Casting [5]

The proposed system works in two steps. In the first step, a high cooling rate is achieved to cool the work chamber from the room temperature to the desired working temperature of -20 to -25°C. In the second step, a lower cooling rate is maintained to sustain the work chamber's temperature. The temperature vs time characteristics of the system is shown in Fig. 3. Since more than one mode of cooling is being used, the authors term the proposed system as *Multimodal Freezing System (MFS)*.

To achieve the different cooling rates, it is proposed to use CO_2 injection system to rapidly cool the chamber to -20 °C, followed by the Vapour Compression Refrigeration (VCR) system for sustained cooling of the chamber at a constant temperature. VCR is a widely available, popular cooling system due to its high efficiency and cost-effectiveness. CO_2 gas is inexpensive and readily available in the bottled form.

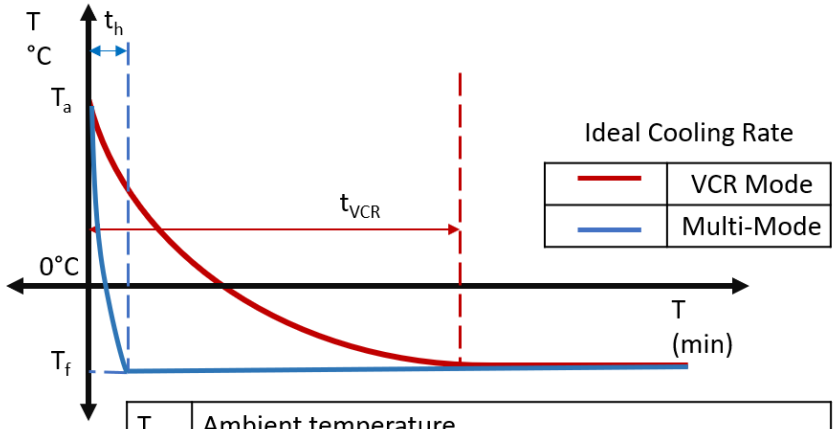

T_a	Ambient temperature
T_f	Temperature of the freezer cabinet (Work envelope)
t_{VCR}	Time to reach temperature T_f for VCR system
t_h	Time to reach temperature T_f for Hybrid system

Fig. 3 Cooling Rates Achieved by the MFS

2. Description of the Multimodal Freezing System

Fig. 4 shows the schematic diagram of the multimodal freezing system. The evaporator coils and CO_2 inlet are located in the freezing chamber.

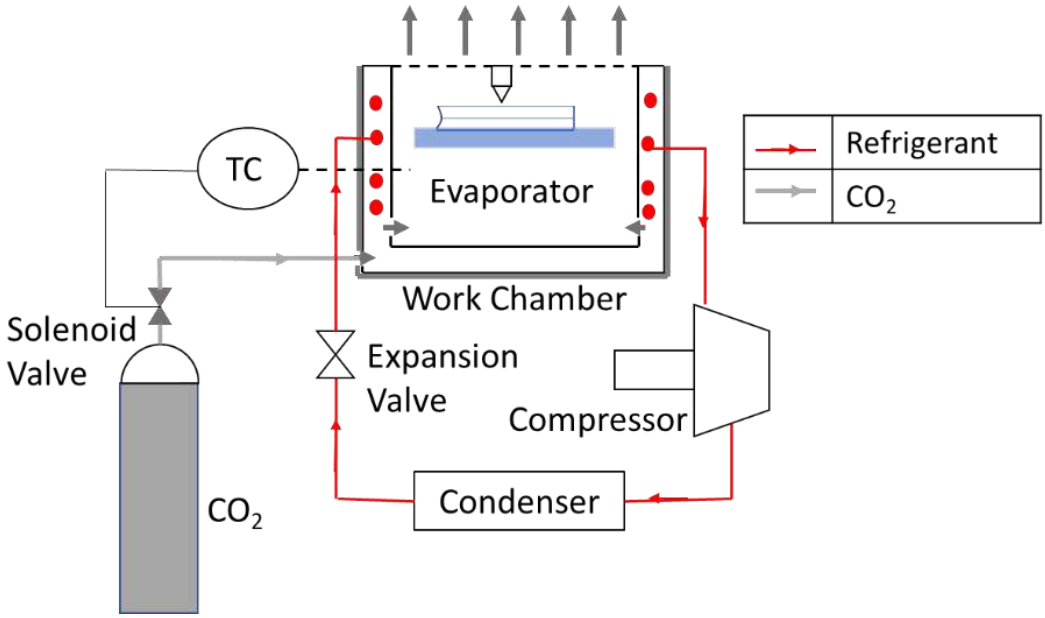

Fig. 4 Schematic Diagram of Multimodal Freezing System

2.1.The architecture of the working chamber

As shown in Fig. 5 (a), (b) and (c), the working chamber walls are made of Polyurethane foam (PUF) of thickness 80 mm lined with a stainless steel sheet from the outer surface. The work platform of area 200 mm x 200 mm and thickness 10 mm is attached to the freely movable platform with four support rods. The stepper motor operated platform moves the table up and down inside the freezing chamber. The motion system is properly insulated against the sub-zero temperatures. The chamber is covered with the bellows at the top (see Fig. 5(a) and 4(b)). The printhead is a delicate part with several micro-nozzles. It is exposed to the sub-zero temperatures. It may result in freezing of water inside the nozzles, choking them up. A heater is used to maintain the temperature of the nozzle plate above freezing point. The details of the set up are mentioned in the section 4.

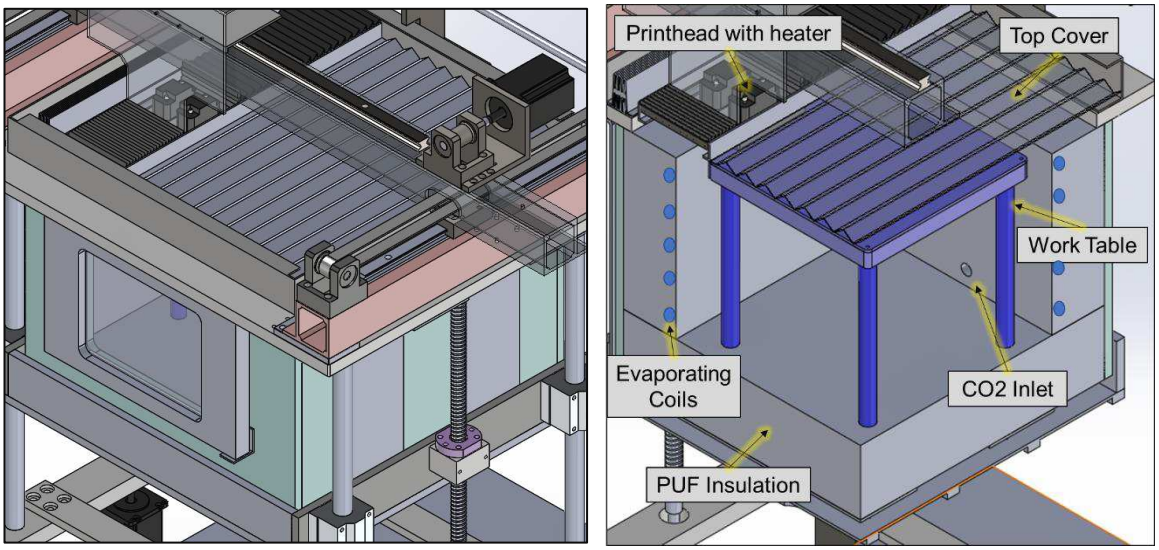

(a) Insulated Work Chamber (b) Section View of the Work Chamber

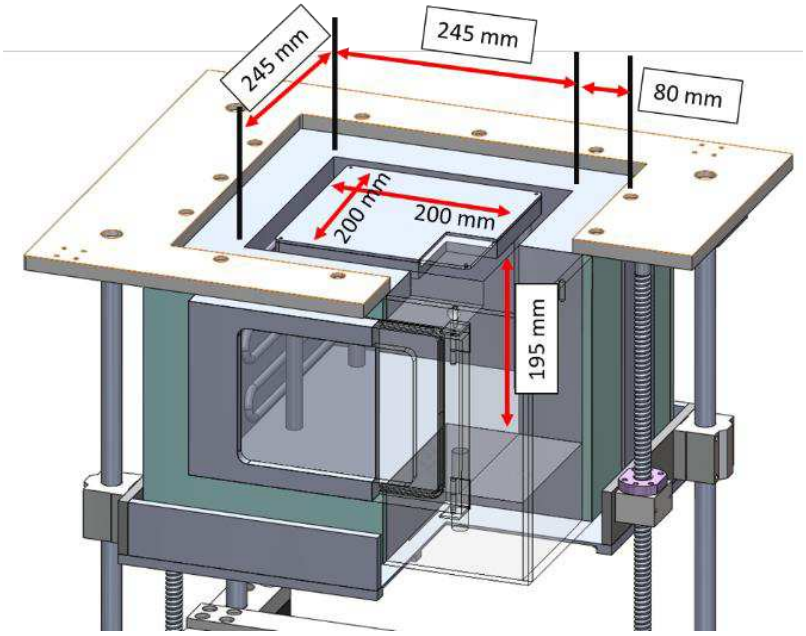

(c) Dimensions of the Work Chamber (Section View)

Fig. 5 Architecture of the Freezing System

2.2.Cooling load estimation

Total cooling load Q_{Total} comprises of five different parts, as shown in table 1. Static cooling loads are single-time cooling loads that arise in step 1 (A and B). Continuous cooling loads arise in step 2, where sustained cooling is required for freezing the water and minimize the heat from the nozzle heater (C,D and E). The ambient temperature is 35°C, and the process temperature is -20°C.

Table 1 Description of the cooling loads

Sl. No.	Item	Description	Load
A	Components of the chamber (aluminium): Work platform (1141 g) Motion system rods (152.5 g each)	$Q_A = C_{p_{Al}} \Delta T \ (m_{wp} + 4 \times m_{rod})$ $C_{p_{Al}}$: 0.887 kJkg^{-1}K^{-1} ΔT : 55 °C m_{wp}: 1305 g m_{rod}: 152.5 g	93.356 kJ
B	Chamber medium (air)	$Q_B = m_{air} C_{p_{air}} \Delta T$ kJ m_{air}: 0.017 kg $C_{p_{air}}$: 1 kJkg^{-1}K^{-1}	0.95 kJ
C	Inlet water	$Q_C = \dot{m}_w (C_{p_w} \Delta T + L)$ kW $\dot{m}_w$: 0.0015 gs^{-1} C_{p_w}: 4182 Jkg^{-1}K^{-1} L: 334 Jg^{-1}	0.00081 kW
D	Heater for nozzles	$Q_D = q \ kW$ ~~Strip~~ Film heater of 10 W	0.010 kW
E	Air infiltration (Assumed 10% of the continous load)	$Q_E = 0.1 \ (Q_C + Q_D)$	0.0015 kW

$$Q_{Total} = Q_A + Q_B + Q_C + Q_D + Q_E \quad (1)$$

3. Mathematical formulation

The objective of the mathematical formulation is to determine the time required for cooling the components.

3.1.CO_2 system

In the proposed multimodal freezing system, the CO_2 system is used for the workspace's initial cooling. Initial cooling is required for to A and B part of the cooling load. CO_2 inlet is inside

the chamber. The isenthalpic expansion of the CO_2 brings about the Joule-Thomson cooling effect. The drop in the temperature due to pressure drop can be determined with equation 2.

$$\Delta T = \mu_{JT} \Delta P \tag{2}$$

In equation 2, μ_{JT} is the Joule-Thomson coefficient. μ_{JT} is 13 K $(MPa)^{-1}$ for CO_2 [11]. For the pressure drop of the 5 MPa in the given case, the temperature change is 65°C, i.e. at the outlet, the temperature is -30°C.

The cooling capacity offered by CO_2 can be calculated using equation 3. CO_2 gas is converted to solid particles (dry ice) during expansion, but the percentage of the dry ice formation is as low as 2% [12]. It can be neglected as the CO_2 system is used only for a short duration. Specific isobaric heat capacity for CO_2 at -30°C and atmospheric pressure is 0.798 KJ $kg^{-1}K^{-1}$.

$$\dot{Q_{CO_2}} = \dot{m_{CO_2}} C_{p_{co2}} (T_2 - T_1) \tag{3}$$

The orifice condition determines the flow rate as per equation 4[12].

$$\dot{m}_{choked} = CA \sqrt{\kappa \rho \, P_{up} \left(\frac{2}{\kappa + 1}\right)^{\frac{\kappa+1}{\kappa-1}}} \tag{4}$$

Table 2 Geometrical and flow parameters for CO_2 system

Notation	Description	Value
C	Dimensionless discharge coefficient	0.81
A	Area of the orifice (m^2)	1.2661×10^{-4}
κ	Dimensionless ratio of the heat capacities at constant pressure to constant volume [12]	1.29
ρ	Gas density (kgm^{-3})	159
P_{up}	Upstream pressure (MPa)	6

$$\dot{m}_{choked} = 0.0021 \; kgs^{-1}$$

It is assumed that CO_2 immediately replaces the air inside the chamber at -30°C, thus, cooling of chamber air can be neglected. Heat transfer is predominantly convective. Convective coefficient is found out from the Nusselt number (Nu) correlation (Equation5).

As per Dittus-Bolter correlation [13],

$$Nu = 0.664 \sqrt{Re} \sqrt[3]{Pr} \tag{5}$$

Where $Re<10^5$, $0.6 < Pr < 2000$

The Nusselt number correlation gives the heat transfer coefficient of 236.25 W m^{-2} K^{-1}. With the given heat transfer coefficient, the heat transfer rate can be determined by Equation 6.

$$\dot{Q}_1 = h_{co2} A_{plate} \Delta T \tag{6}$$

The heat transfer rate in the CO_2 system is 1.06 kW; thus, it takes 88 s to cool the work platform to -20°C.

3.2.Vapour Compression Refrigeration (VCR) system

In the VCR system, the first heat transfer occurs from the chamber medium (air) to evaporator coils and then from the work platform to the chamber medium. Fig. 6 shows a typical VCR cycle where process 1-2 is compression, 2-3 is isobaric condensation, 3-4 is the isenthalpic expansion, and 4-1 is evaporation.

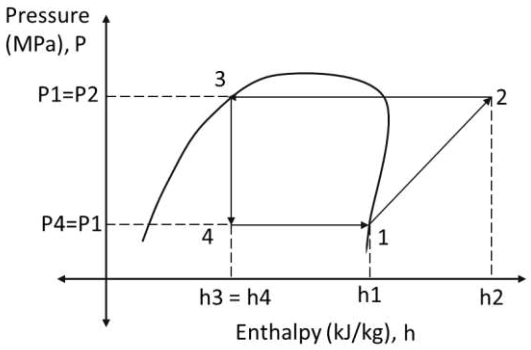

Fig. 6 P-h Diagram for the VCR Cycle

The enthalpy of the refrigerant is the function of the saturation temperature (equation 7)[14]. Enthalpy of the refrigerant at various temperatures can be expressed with the empirical relations given by equations 8 and 9.

$$h = f(T_s) \tag{7}$$

$$h_{sl} = a_1 + a_2 T_{sl} + a_3 T_{sl}^2 + a_4 T_{sl}^3 \tag{8}$$

$$h_{sv} = b_1 + b_2 T_{sv} + b_3 T_{sv}^2 + b_4 T_{sv}^3 \tag{9}$$

T_s (°C) is saturation temperature, a_1, a_2, a_3, a_4 and b_1, b_2, b_3, b_4 are coefficients, h_{sl} and h_{sv} are the enthalpies of the refrigerants in the saturated liquid and vapor conditions. T_{sl} (°C) and T_{sv} (°C) are the saturated liquid and vapor temperatures of the refrigerant[15].

As per the ASHRAE enthalpy datum, the enthalpy polynomial coefficients for saturated liquid R134a are expressed by equation 10 [13]. Equation 7 helps to predict the enthalpy data with ±0.2 kJ kg^{-1} accuracy for the temperature range -40°C to 70°C, which is within the present range of the study. Here, T_l is the liquid temperature of the refrigerant where $\Delta T_b = T_{sat} - T_l$(°C) ≥0.

$$h_l = 50952 + 1335.29\, T_l + 1.70650\, T_l^2 + 7.6741 \times 10^{-3} T_l^3 \quad (\text{Jkg}^{-1}) \tag{10}$$

The saturation liquid temperature for the refrigerant is measured after 32°C.

$$h_l = 95.6802\ kJ/kg$$

Similarly, the ASHRAE enthalpy datum for saturated vapor can be predicted with the equation 11 [15], where T is defined in °C.

$$h_{sv} = 249455 + 606.163\, T_{sv} - 1.05644\, T_{sv}^2 - 1.82426 \times 10^{-2} T_{sv}^3 \quad (\text{Jkg}^{-1}) \tag{11}$$

As the compression is isentropic, the saturation temperature can be assumed evaporation temperature of the refrigerated enclosure, i.e., -23.3 °C.

$$h_{sv} = 234.988\ KJkg^{-1}$$

For superheated vapor, the enthalpy datum can be calculated with equation 12 [15]. Here, T_s is the superheat temperature and $\Delta T_s = T_s - T_{sat}$.

$$\begin{aligned} h_{sup} = h_{sv}\,(1 + 3.48186\ \times 10^{-3}\Delta T_s + 1.6886 \times 10^{-6}{\Delta T_s}^2 \\ + 9.2642 \times 10^{-6}\Delta T_s T_{sat} - 7.698 \times 10^{-8}{\Delta T_s}^2 T_{sat} \\ + 1.7070 \times 10^{-7}\Delta T_s\,{T_{sat}}^2 - 1.2130 \times 10^{-9}\,{\Delta T_s}^2\,{T_{sat}}^2) \end{aligned} \quad (12)$$

The superheated temperature (T_s) is 54.4°C, and the evaporation of the refrigerant occurs at -23.3°C. The refrigerant used is R134a. The gas pressure after compression is found to be 1.35 MPa, the corresponding saturation temperature (T_{sat}) is found to be 50.953°C.

h_{sup} is expressed as KJ/kg where temperatures are expressed in degree Celsius.
Where $\Delta T_s = T_s - T_{sat}$ = 54.4 – 50.95 = 3.45 °C

Hence,

$$h_{sup} = 238.5520\ KJkg^{-1}$$

Compressor work:

$$W = h_{sup} - h_{sv} \quad (13)$$

$$W = 3.564\ \text{kJkg}^{-1}$$

Total refrigeration effect:

$$RE = h_{sv} - h_{sl} \quad (14)$$

$$RE = 139.3078\ KJkg^{-1}$$

For small compartment cooling applications, a compressor with a cooling capacity of 281 W is selected. The mass flow rate capacity of the compressor is 36 gs^{-1}.

If VCR alone were used, the time required to handle the load A and B and cool the system to -20 °C would be higher than that of the CO_2 system.

$$\dot{Q}_2 = h_{coil} A_{coil} (T_2 - T_1) \tag{15}$$

Where *h* is the heat transfer coefficient, *A* is the surface area of the heat exchange and T_2 is evaporator coil temperature and T_1 is the air temperature. The value of *h* can be estimated by using the Nusselt number correlation for the cylindrical tube (equation 16)[16]. The heat transfer coefficient is 3.07 $Wm^{-2}K^{-1}$. Thus, equation 15 yields the value of heat transfer rate Q_2 as 0.016 kW. Therefore, if we use VCR for part A and B of the cooling load, it takes 97.23 min for chamber medium (air) to reach the desired temperature.

$$Nu = \left\{0.6 + \frac{0.387 Ra^{1/6}}{[1 + (0.559/Pr)^{9/16}]^{8/27}}\right\}^2 \tag{16}$$

The *h* is calculated based on the equation (18) for the plate heat transfer, and found to be 0.46 $Wm^{-2}K^{-1}$ [17]. The heat transfer rate between the chamber medium and the work platform is given by equation 17. The combined effect of $\dot{Q}_2$ and $\dot{Q}_3$ determines the total time taken for the cooling of the work platform. The time is determined with numerical study subsequently.

$$\dot{Q}_3 = h_{plate} A_{plate} (T_2 - T_1) \tag{17}$$

$$Nu = 0.27\ (Gr\ .\ \mathrm{Pr})^{0.25} \tag{18}$$

The results of the mathematical analysis have been correlated and discussed in the section 5.

4. Experimental setup and numerical procedure

The time to reach the target temperature is predicted by mathematical analysis as 88 s (work platform) and 97 min (chamber medium) for the CO_2 system and VCR system. The experimental and numerical study is carried out to ascertain the time.

4.1.Experimental setup

The experimental setup, as shown in Fig. 7 (a), consists of an insulated chamber with the side opening door. The chamber's top portion is covered with an X-Y motion bellow that provides a cover while enabling the material deposition head's motion in the X and Y directions. Evaporator coils are positioned around the chamber walls uncovered to increase the heat transfer efficiency as shown in Fig. 7 (b). Thermocouple measures the temperature variation (Fig. 7 (c)). A 10 W polyimide foil heater is sandwiched between the nozzle plate and the base plate as shown in Fig. 7 (d). Foil heater is used for maintaining the nozzle plate at 60° C that prevents the nozzles from freezing. Experiments show that the nozzle plate maintained at 60° C is effective in keeping the nozzles warm without melting the uppermost frozen layer of ice.

(a) Enclosed Work Chamber

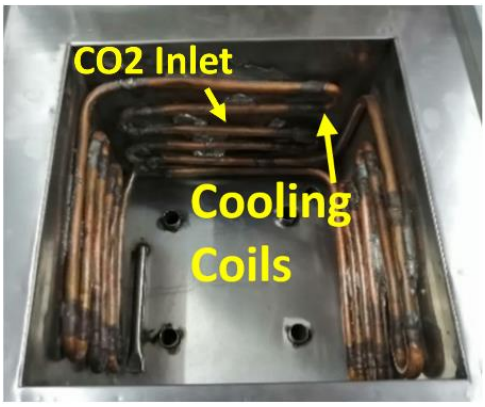

(b)Interior of the Chamber

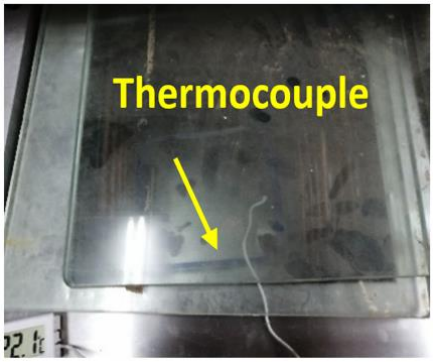

(c) Thermocouple

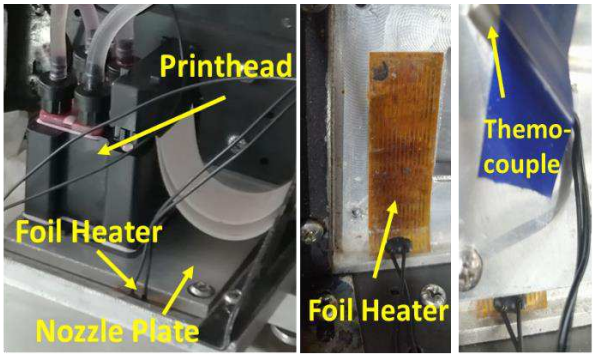

(d) Nozzle Heater Arrangement

Fig. 7 Experimental setup for the multimodal cooling system

CO_2 is released in the chamber, and the temperature is recorded using a K-type thermocouple. The change in the temperature is measured every 5 seconds as the temperature changes rapidly. Similarly, the VCR system is tested, and the temperature is noted after every

2 minutes as the change in the temperature is slow. The observations of the experiment are mentioned in Fig. 8.

Uncertainty of measurement

The sensitivity of the measuring instruments gives rise to the variation in the measured values. The measurement errors are addressed in table 3.

Table 3 Uncertainty of measurement

Sl. No.	Quantity	Absolute Value	Uncertainty
1	Chamber length	245 mm	±0.01 mm
2	Width	245 mm	±0.01 mm
3	Height	195 mm	±0.01 mm
4	CO_2 inlet hole	12.7 mm	±0.01 mm
5	Temperature	36 °C	±1.1 °C
6	Pressure	60 Bar	±0.5 Bar

4.2.Numerical methodology

Three-dimensional numerical simulations are carried out for the multimodal system using flow simulation CFD package by Solidworks® available commercially. The software solves the Navier-Stokes equations that are formulations of mass, momentum, and energy conservation(Solidworks Flow Simulation Technical Reference, 2012).

Conservation of mass:

$$\frac{\partial \rho}{\partial t} + \frac{\partial (\rho u_i)}{\partial x_i} = 0 \tag{19}$$

Conservation of momentum:

$$\frac{\partial (\rho u_i)}{\partial t} + \frac{\partial}{\partial x_j}\left(\rho u_i u_j\right) + \frac{\partial P}{\partial x_i} = \frac{\partial}{\partial x_j}\left(\tau_{ij} + \tau_{ij}^{R}\right) + S_i \tag{20}$$

Conservation of energy:

$$\frac{\partial \rho H}{\partial t} + \frac{\partial \rho u_i H}{\partial x_i} = \frac{\partial}{\partial x_i}\left(u_j\left(\tau_{ij} + \tau_{ij}^R\right) + q_i\right) + \frac{\partial P}{\partial t} - \tau_{ij}^R \frac{\partial u_i}{\partial x_j} + \rho\varepsilon + S_i u_i + Q_H \quad (21)$$

Standard $k-\varepsilon$ turbulence model:

Turbulent Kinetic Energy (k)

$$\frac{\partial(\rho k)}{\partial t} + \frac{\partial(\rho u_i k)}{\partial x_i} = \frac{\partial}{\partial x_i}\left(\left(\mu + \frac{\mu_t}{\sigma_k}\right)\frac{\partial k}{\partial x_i}\right) + \tau_{ij}^R \frac{\partial u_i}{\partial x_j} - \rho\varepsilon + \mu_t P_B$$

Turbulent Dissipation (ε)

$$\frac{\partial(\rho\varepsilon)}{\partial t} + \frac{\partial(\rho u_i \varepsilon)}{\partial x_i} = \frac{\partial}{\partial x_i}\left(\left(\mu + \frac{\mu_t}{\sigma_\varepsilon}\right)\frac{\partial \varepsilon}{\partial x_i}\right) + C_{\varepsilon_1}\frac{\varepsilon}{k}\left(f_1 \tau_{ij}^R \frac{\partial u_i}{\partial x_j} + \mu_t C_B P_B\right) - C_{\varepsilon_2} f_2 \frac{\rho\varepsilon^2}{k}$$

Where, $H = h + \frac{u^2}{2}$ and is ρ density of the fluid, u_j, u_j are the velocity components, x, y and z are the coordinates, τ_{ij} is the viscous shear stress tensor, P is the pressure, H is the total energy, q_i is the diffusive heat flux, Q_H is the heat source or sink per unit volume, ε is the rate of dissipation of the turbulent kinetic energy, S_i is the summation of mass distributed external force per unit mass due to porous media, gravity, and rotation where $S_i = S_i^{porous} + S_i^{gravity} + S_i^{rotation}$, h is the thermal enthalpy. Subscripts denote the summation over three coordinates. δ_{ij} is the Kronecker delta function, P_B is turbulent generation due to buoyancy, μ_t is turbulent eddy viscosity, μ is dynamic viscosity, f_1 and f_2 are viscosity factors, C_{ε_1}, C_{ε_2}, σ_ε, σ_k are constants defined empirically.

The geometry is as shown in Fig. 8. An adaptive meshing approach is used. The results of the grid independence study are shown in table 4. The minimum temperature after 60 s is recorded for the CO_2 system and after 3600 s for the VCR system. After 85,000 cells, the temperature variation is minimal (0.03% and 0.1% for CO_2 and VCR systems, respectively).

Table 4 Grid independence study for the numerical simulation

Number of cells	CO2 System		VCR system	
	Temperature	% deviation	Temperature	% deviation
65,000	0.6918	12.02	33.6916	3.34
85,000	0.6086	0.03	32.5659	0.10
90,000	0.6084		32.5329	

For CO_2 system simulation, the inlet is set up as a pressure inlet with a total pressure of 60 bar, and the outlet is set up as a pressure outlet with environmental pressure, 1.013 bar. The surface goals for the worktable surface are set as minimum solid temperature. The heat transfer coefficient is assigned as 236 $Wm^{-2}K^{-1}$ for the worktable surface (Ref - section 3.1). The work chamber walls are considered ideal walls. (see Fig. 8)

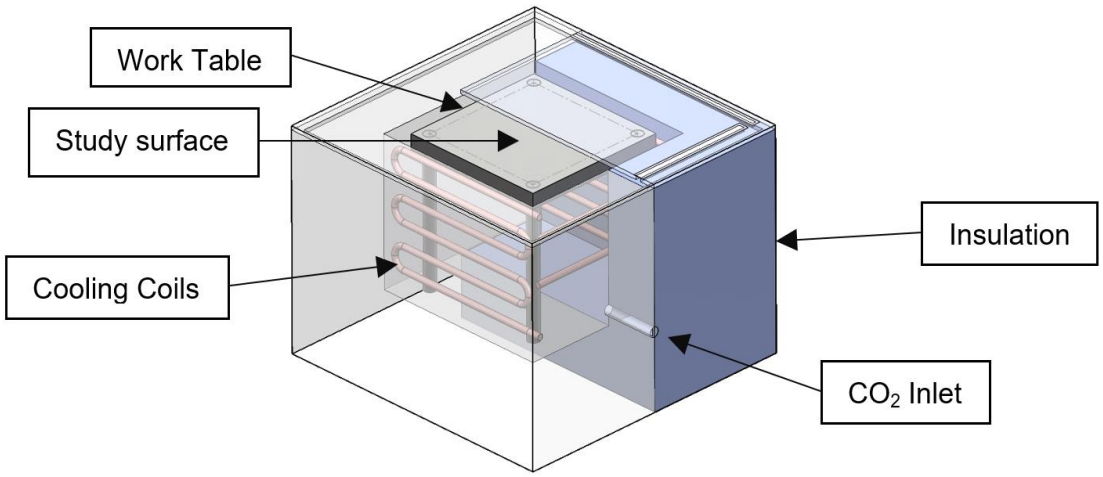

Fig. 8 Section View of the Geometry for the Simulation

For the VCR system, the geometrical and flow parameters are mentioned in table 5. Since it is a natural convection problem, the h values for the cooling coil and the work surface are estimated as 3.07 and 0.48 $Wm^{-2}K^{-1}$, as mentioned in section 3.2. The minimum cooling coil temperature obtained by the VCR system at the evaporator is -23.3°C. The work chamber walls are considered ideal walls. (see Fig. 7). The temperature is recorded for the study surface. The results are mentioned in Fig. 8.

Table 5 Geometrical and flow parameters considered for the simulation

Sl. No	Parameter	Range
1	Volume	245 mm x 245 mm x 195 mm
2	CO2 Inlet	12.7 mm (0.5”)
3	CO_2 cylinder pressure	60 Bar (6 MPa)
4	VCR system compressor	Emerson make (Product: KCN411LAG-B234H)
5	Copper tube size	8 x 6 mm

6	Refrigerant	R 134a
7	Condenser	Air-cooled, 558.8 mm x 482 mm (22” x 19”)
8	Ambient temperature	35 °C (308 K)
9	Work chamber target temperature	-20°C (243 K)

5. Results and discussion

The results show the temperature vs time characteristics of the CO_2 and VCR systems. The temperature profiles of the chamber are also plotted for different time instances.

5.1 Variation of the temperature with time

Fig. 9 shows the temperature-time graph obtained by the numerical simulation and an experiment of the CO_2 and the VCR system. It is observed that the experimental and numerical results are in agreement with each other. It is observed in Fig. 8 that the target temperature -20°C is obtained in 103 s with the help of the CO_2 system. The VCR system takes 6 hours to reach the same temperature.

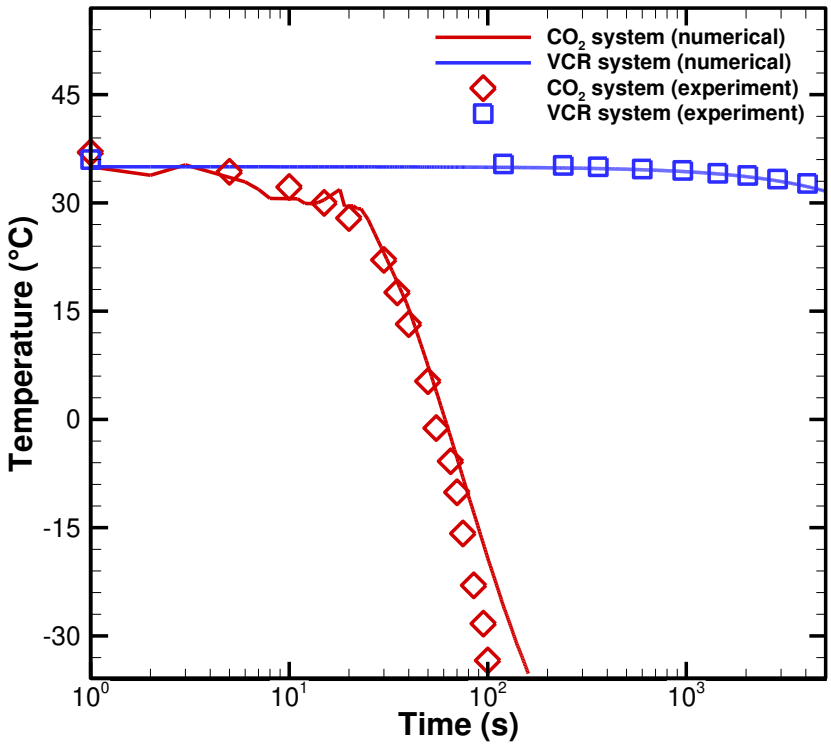

Fig. 9 Time-Temperature Graph for the Multimodal Freezing System

In the CO_2 system, the CO_2 gas acts as a cooling medium and directly exchanges the heat with the work chamber. However, in the VCR system, the heat is first exchanged with the chamber medium (air) and then the cold air exchanges the heat with the chamber contents, i.e. two convective heat transfer coefficients are involved. It results in slower heat transfer as compared to the CO_2 system.

5.2 Temperature profiles

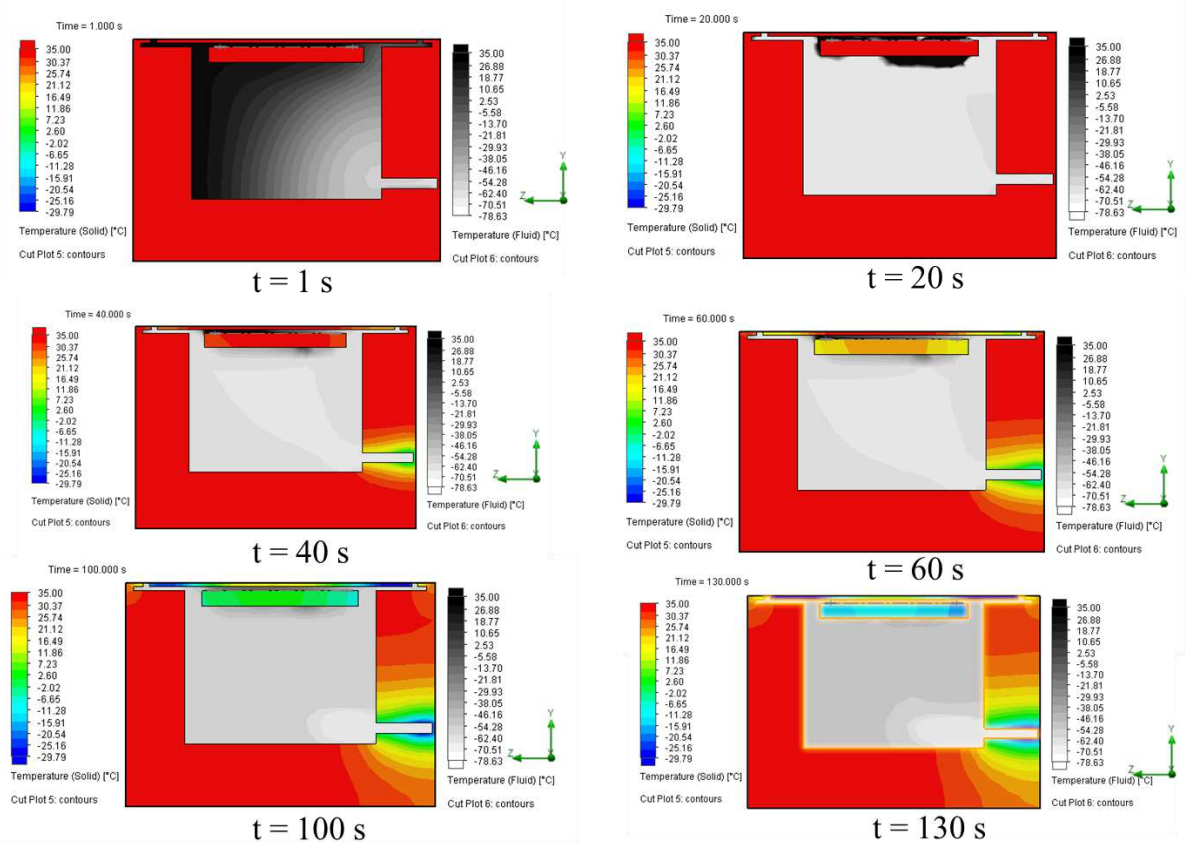

Fig.10 Temperature Profile (Solid and Liquid) for CO_2 System (t=125s)

Fig. 10 shows the temperature contours of the solid parts and the chamber medium fluid (CO_2). It is observed that the temperatures of the CO_2 gas at 130 s range from -18.88 to -78.63 °C and the work platform from -8 to -22°C.

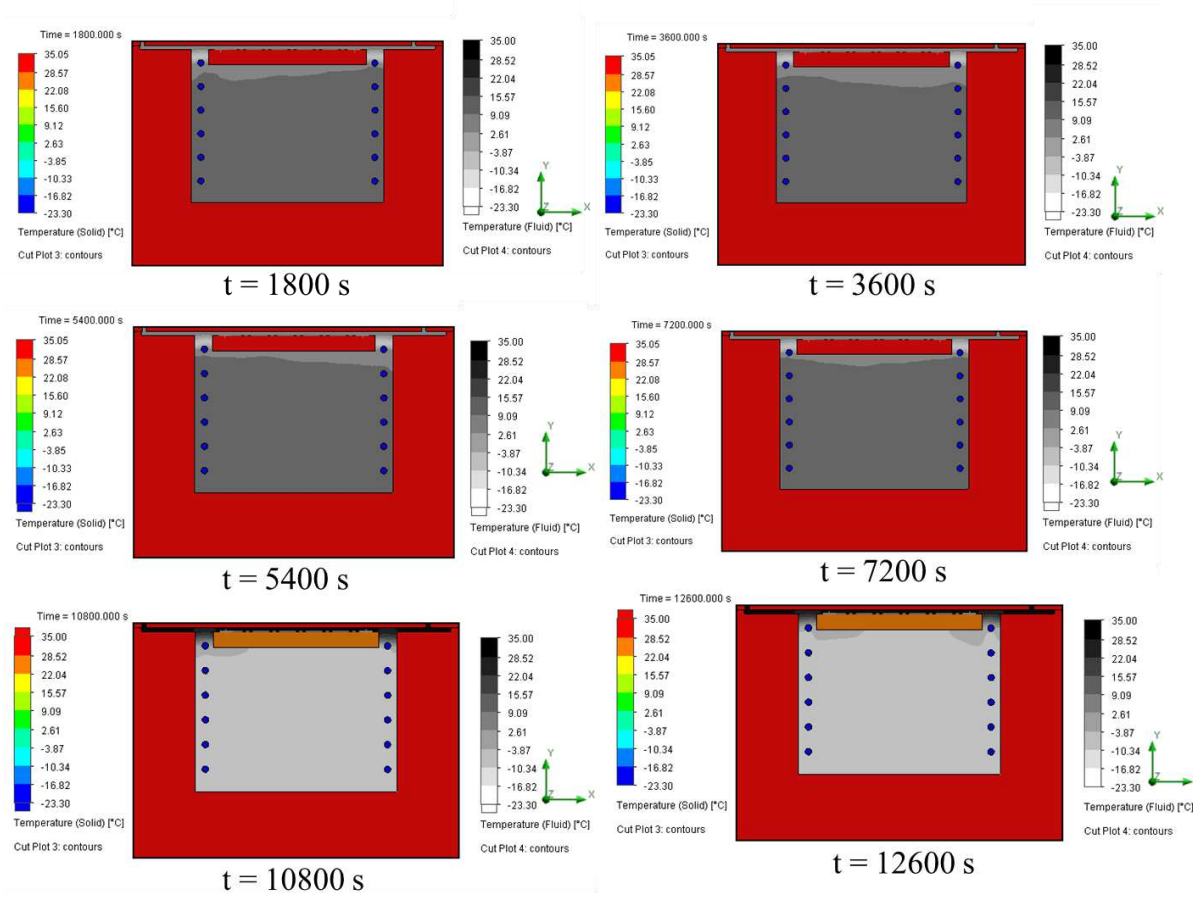

Fig. 11 Temperature Profile (Solid and Liquid) for VCR System (t = 15338 s)

Fig. 11 shows the work platform temperature is in the range of 22.04 to 28.52 °C at 12600 s. Due to the absence of a fan, the cooling process works slow. The experimental results suggest the same.

5.3 Demonstration of the ice 3D printing

Ice structures were 3D printed using the present experimental set up. The model material is demineralized water. Undercut-free prismatic geometries are printed to validate the present system. The 3D printed ice parts are shown in Fig. 12. Fig. 12 (a) shows the CAD model of the embossed letters of the institute's acronym. Fig. 12 (b) is the 3D printed ice part from the CAD model. Fig. 12 (c) shows the CAD model of the ornamental parts such as pendants and Fig. 12 (d) shows the 3D printed ice part.

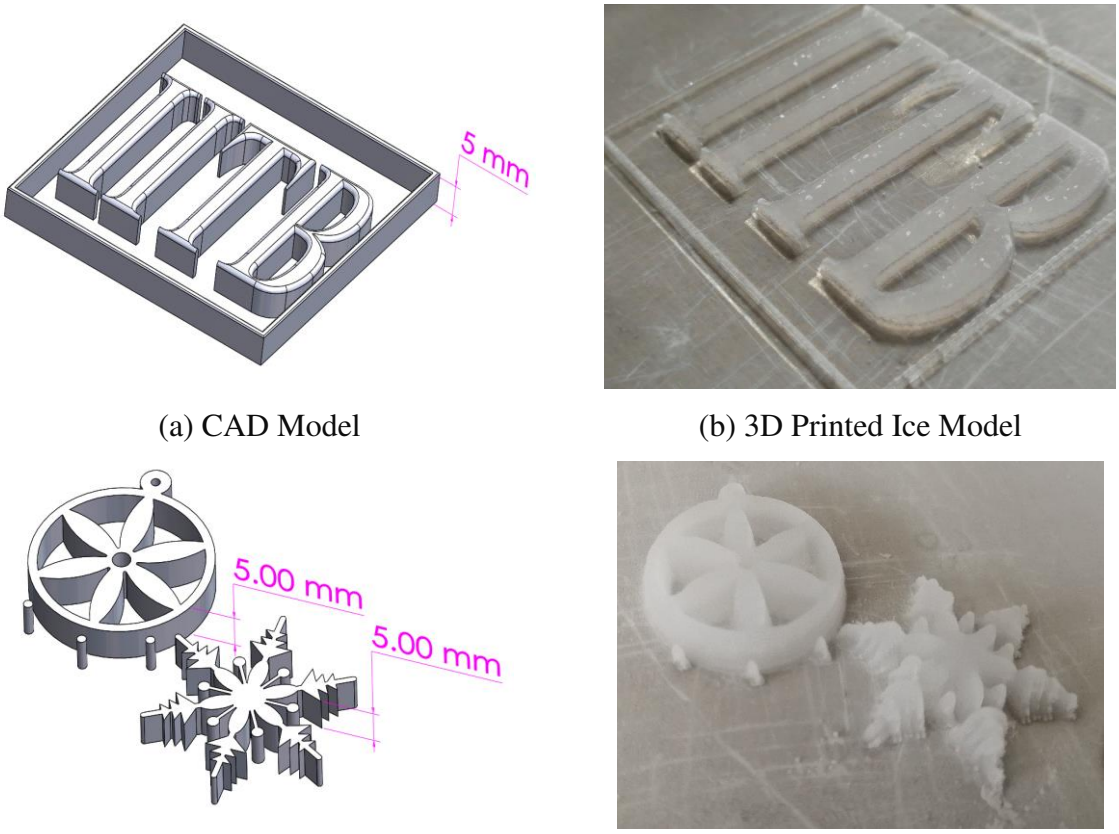

(a) CAD Model (b) 3D Printed Ice Model

(c) CAD Model (d) 3D Printed Ice Model

Fig. 12 3D Printed Ice Parts Using Multimodal Cooling System

6. Conclusion

Following are the merits and demerits of the CO2 based multimodal cooling system.

Merits:

- Multimodal cooling system reduces the cooling time and help cryo-3DP process to start instantly.
- CO_2 is used for a short duration and not for the entire process. It ensures optimum consumption.

Demerits:

- CO_2 is hazardous to the environment. Human safety needs to be assured with appropriate sensors and evacuation system.
- Multimodal system is more complex than the conventional one.

Acknowledgements

The authors wish to acknowledge the help extended by Mr. Abhishek Verma and the team of M/S. Digital Innovations, Indore, India for their help in the experimental work.

Funding - There are no financial conflicts of interest to disclose

Conflicts of interest/Competing interests – Not applicable

Availability of data and material - Not applicable

Code availability - Not applicable

Ethics approval - Not applicable

Consent to participate - Not applicable

Consent for publication - Not applicable

References

[1] W. Zhang, M. C. Leu, Z. Ji, and Y. Yan (1999) Rapid freezing prototyping with water. *Mater. Des.*, vol. 20, no. 2–3, pp. 139–145. https://doi.org/10.1016/S0261-3069(99)00020-5

[2] E. Barnett, J. Angeles, and D. Pasini (2009) Robot-Assisted Rapid Prototyping for Ice Structures. 2009 IEEE International Conference on Robotics and Automation vol. 33, no. 4, pp. 146–151. https://doi.org/10.1109/ROBOT.2009.5152317

[3] F. Zheng, Z. Wang, J. Huang, and Z. Li (2020) Inkjet printing-based fabrication of microscale 3D ice structures, *Microsystems Nanoeng.*, vol. 6, no. 1. https://doi.org/10.1038/s41378-020-00199-x

[4] F. Zheng, J. Huang, and Z. Li (2019) Fabrication of 3D Micro Ice Structures Based on Inkjet Printing, *Proc. IEEE Int. Conf. Micro Electro Mech. Syst.*, pp. 368–371,

http://dx.doi.org/10.1109/MEMSYS.2019.8870837

[5] Q. Liu, G. Sui, and M. C. Leu (2002) Experimental study on the ice pattern fabrication for the investment casting by rapid freeze prototyping (RFP), *Comput. Ind.*, vol. 48, no. 3, pp. 181–197. https://doi.org/10.1016/S0166-3615(02)00042-8

[6] P. Sijpkes, E. Barnett, J. Angeles, and D. Pasini (2009) The architecture of phase change at McGill, *Leadersh. Archit. Res.*, no. April, p. 241. https://doi.org/10.17831/rep:arcc%25y155

[7] J. Jin and Y. Chen (2017) Highly removable water support for Stereolithography, *J. Manuf. Process.*, vol. 28, pp. 541–549. https://doi.org/10.1016/j.jmapro.2017.04.023

[8] H. Zhang, H. Li, M. Wu, H. Yu, W. Wang, and Z. Li (2014) 3D ICE printing as a fabrication technology of microfluidics with pre-sealed reagents, *Proc. IEEE Int. Conf. Micro Electro Mech. Syst.*, pp. 52–55. https://doi.org/10.1109/MEMSYS.2014.6765571

[9] Hong-Ze Zhang, Fang-Ting Zhang, Xiao-Hui Zhang, Dong Huang, Ying-Lin Zhou, Zhi-Hong Li, Xin-Xiang Zhang (2015) Portable, Easy-to-Operate, and Antifouling Microcapsule Array Chips Fabricated by 3D Ice Printing for Visual Target Detection, *Anal. Chem.*, vol. 87, no. 12, pp. 6397–6402. https://doi.org/10.1021/acs.analchem.5b01440

[10] Feng Zhang, Min Wei, Vilayanur V. Viswanathan, Benjamin Swart, Yuyan Shao, Gang Wu, Chi Zhou (2017) 3D printing technologies for electrochemical energy storage, *Nano Energy*, vol. 40, no. August, pp. 418–431. https://doi.org/10.1016/j.nanoen.2017.08.037

[11] A. Mazzoldi, T. Hill, and J. J. Colls (2008) CO_2 transportation for carbon capture and storage: Sublimation of carbon dioxide from a dry ice bank, *Int. J. Greenh. Gas Control*, vol. 2, no. 2, pp. 210–218. https://doi.org/10.1016/S1750-5836(07)00118-1

[12] C. Al Sayed, L. Vinches, and S. Hallé (2018) Experimental Investigation of the Cooling Capacity of Gaseous Carbon Dioxide in Free Jet Expansion for Use in Portable Air-Cooling Systems, *Open J. Appl. Sci.*, vol. 08, no. 02, pp. 62–72.

https://doi.org/10.4236/ojapps.2018.82005

[13] Y. Jaluria (2019) *Design and Optimization of Thermal Systems*. CRC Press.

[14] S. K. Wang (1994) *Handbook of air conditioning and refrigeration*. McGraw Hill.

[15] A. C. Cleland (1994) Polynomial curve-fits for refrigerant thermodynamic properties: extension to include R134a, *Int. J. Refrig.*, vol. 17, no. 4, pp. 245–249. https://doi.org/10.1016/0140-7007(94)90040-X

[16] S. W. Churchill and H. H. S. Chu (1975) Correlating equations for laminar and turbulent free convection from a horizontal cylinder. *Int. J. Heat Mass Transf.*, vol. 18, no. 9, pp. 1049–1053. https://doi.org/10.1016/0017-9310(75)90222-7

[17] C. P. Kothandaraman (2006) *Fundamentals of Heat and Mass Transfer*. New Age International Publishers.

[18] Solidworks Flow Simulation Technical Reference (2012), SolidWorks Online Archives, https://d2t1xqejof9utc.cloudfront.net/files/18565/SW_CFD_technical_reference.pdf?1361897013 Accessed 10 February 2021

Figures

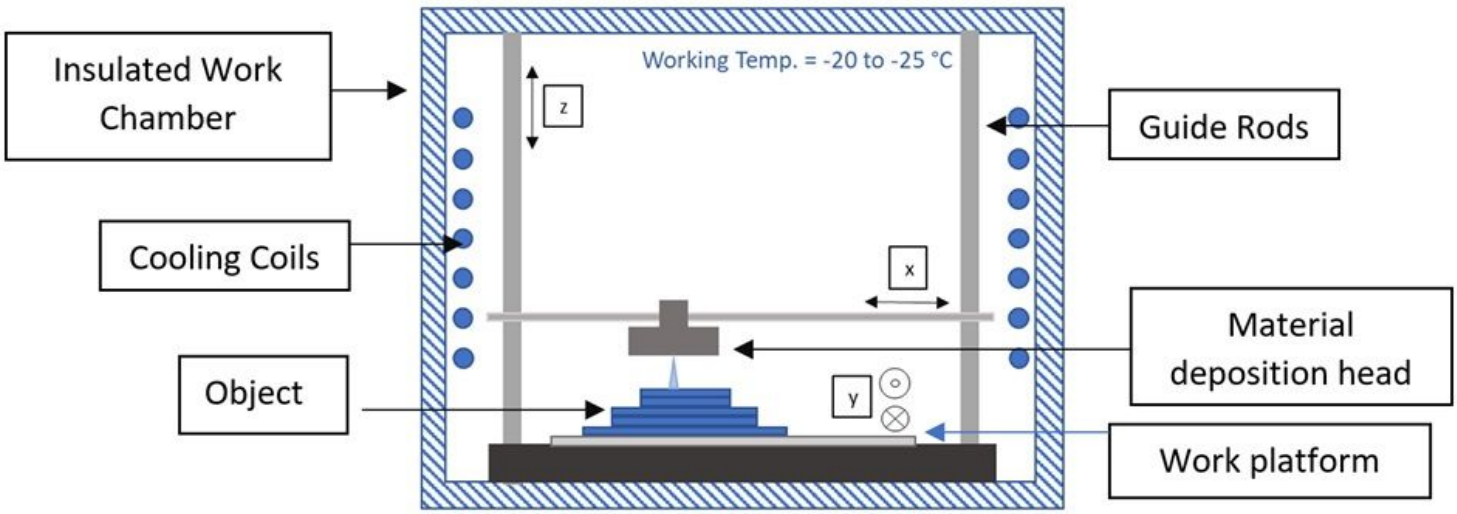

Figure 1

Schematic diagram of a cryogenic 3D printer

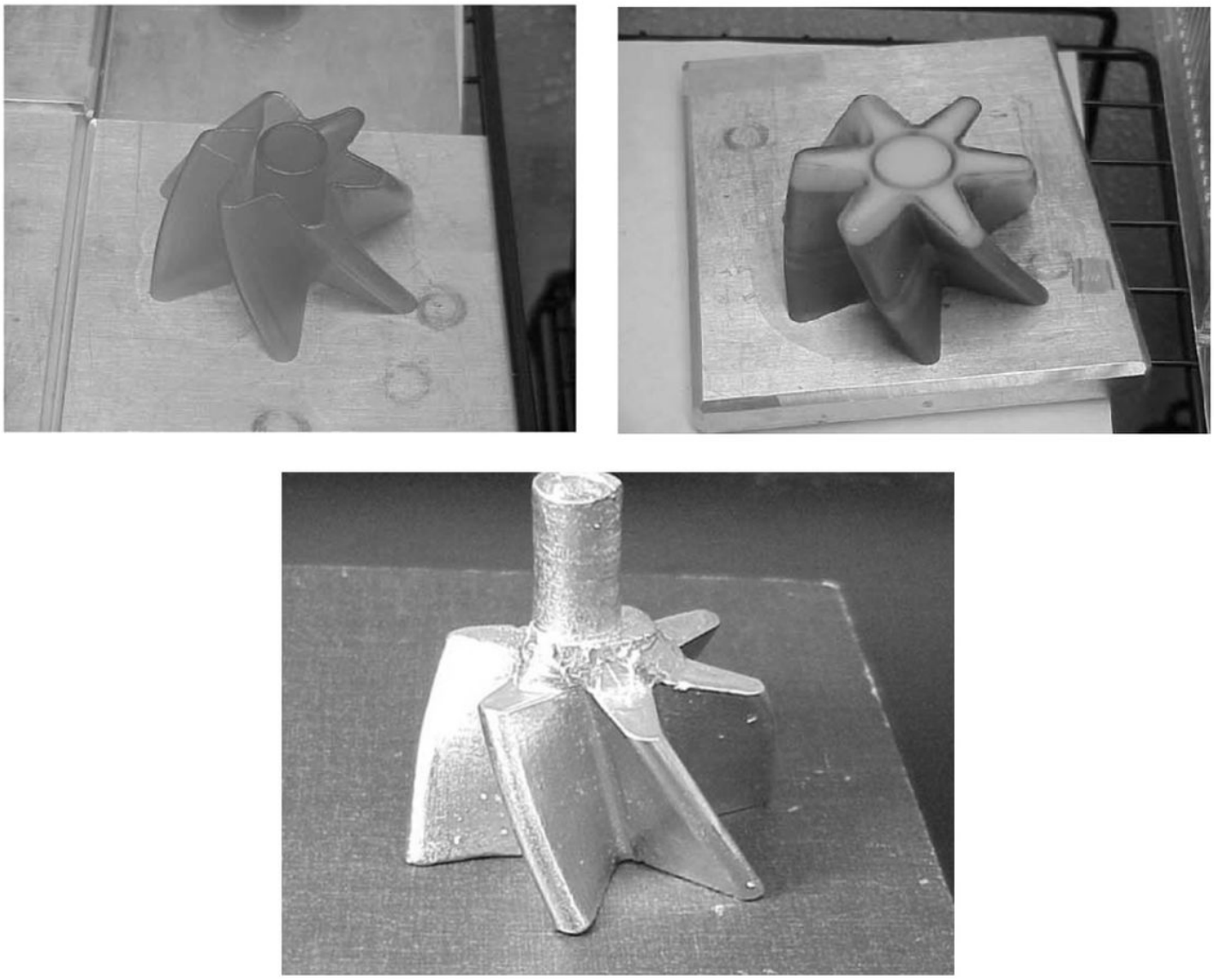

Figure 2

Cryo-3DP of ice : Ice as a pattern for investment casting (Liu et al., 2002). (a) 3D Printed ice boundary. (b) Block of ice as a pattern. (c) Cast part.

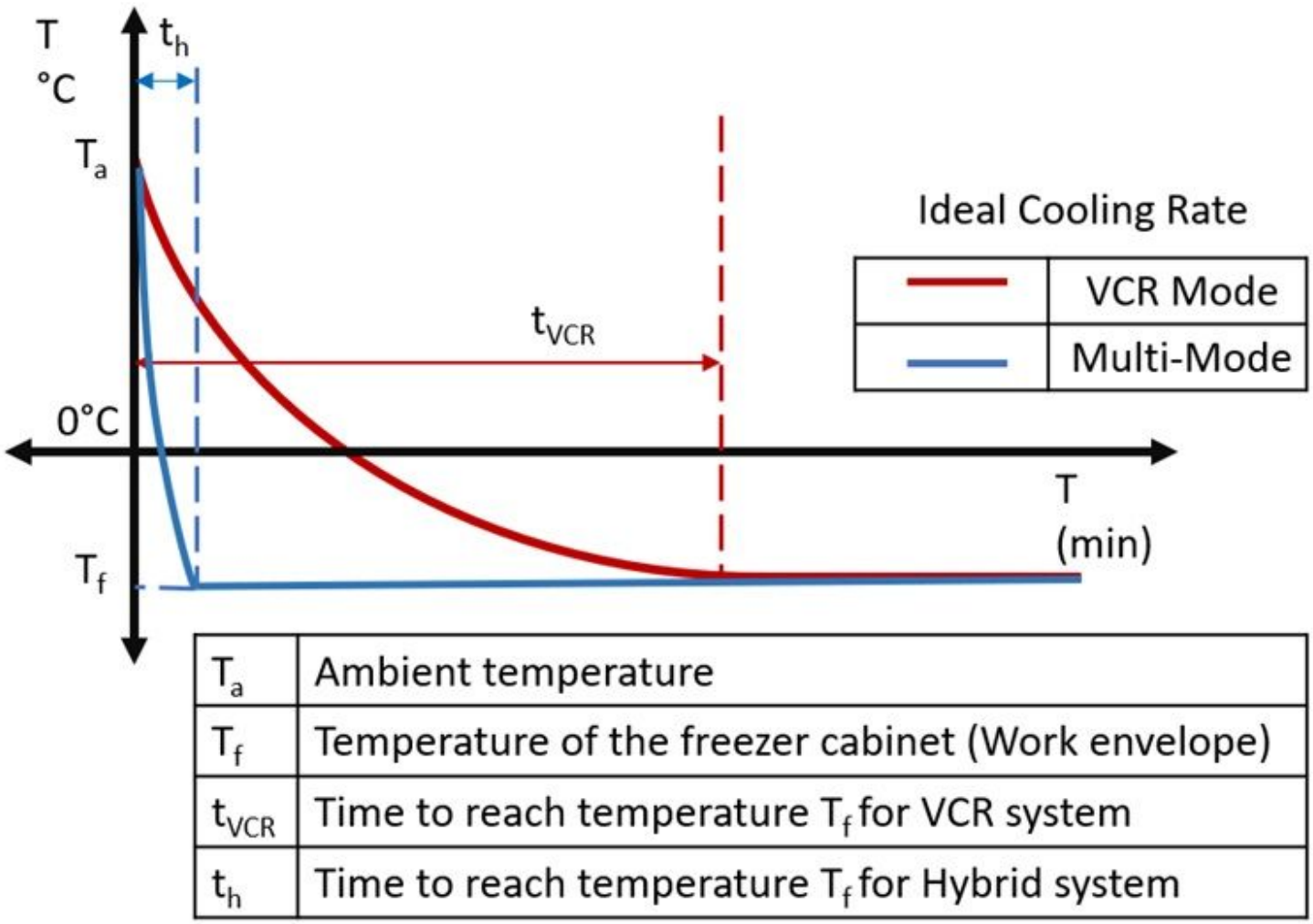

T_a	Ambient temperature
T_f	Temperature of the freezer cabinet (Work envelope)
t_{VCR}	Time to reach temperature T_f for VCR system
t_h	Time to reach temperature T_f for Hybrid system

Figure 3

Proposed cooling rates by CO2 system and Vapor Compression Refrigeration (VCR)

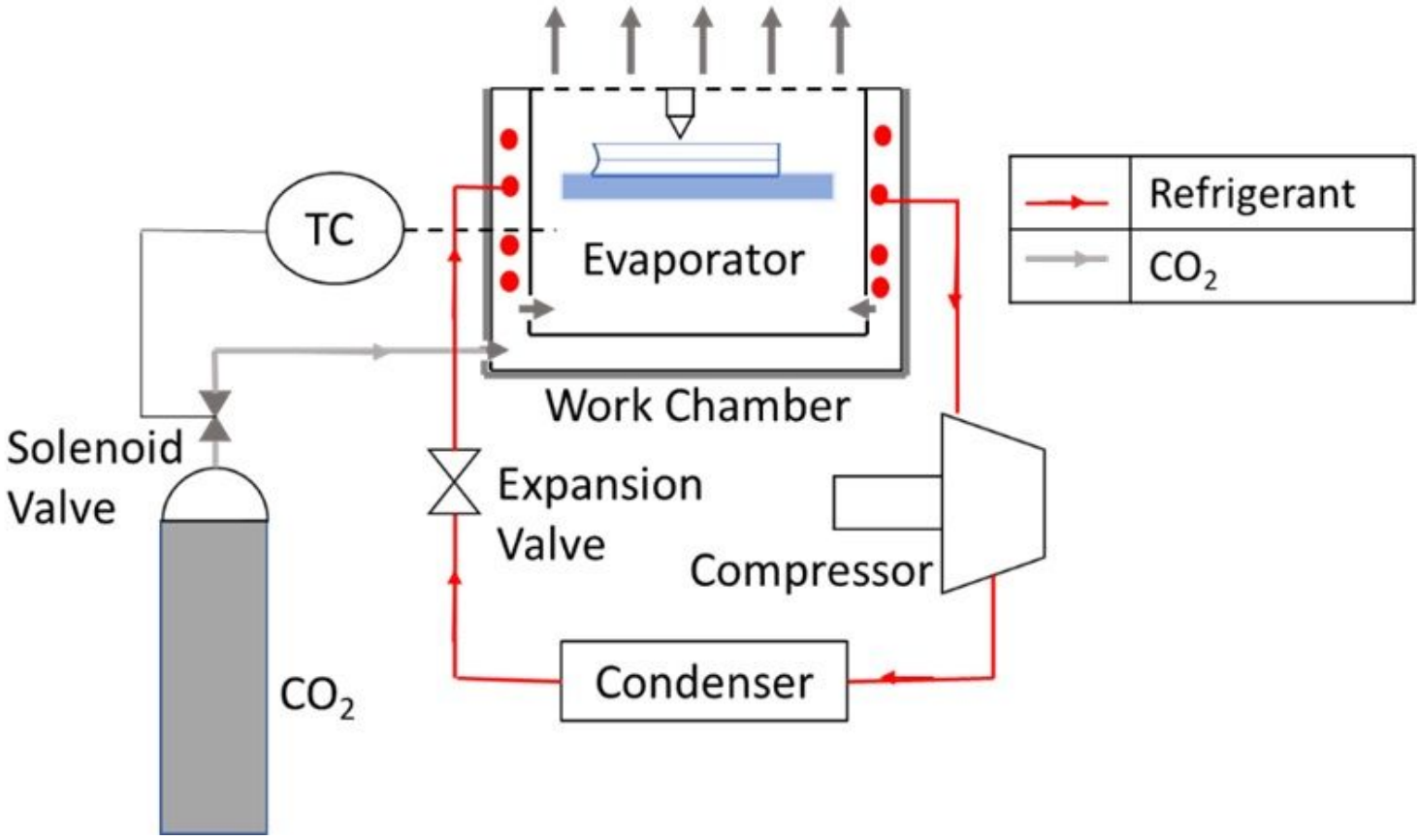

Figure 4

Schematic diagram of multimodal freezing system

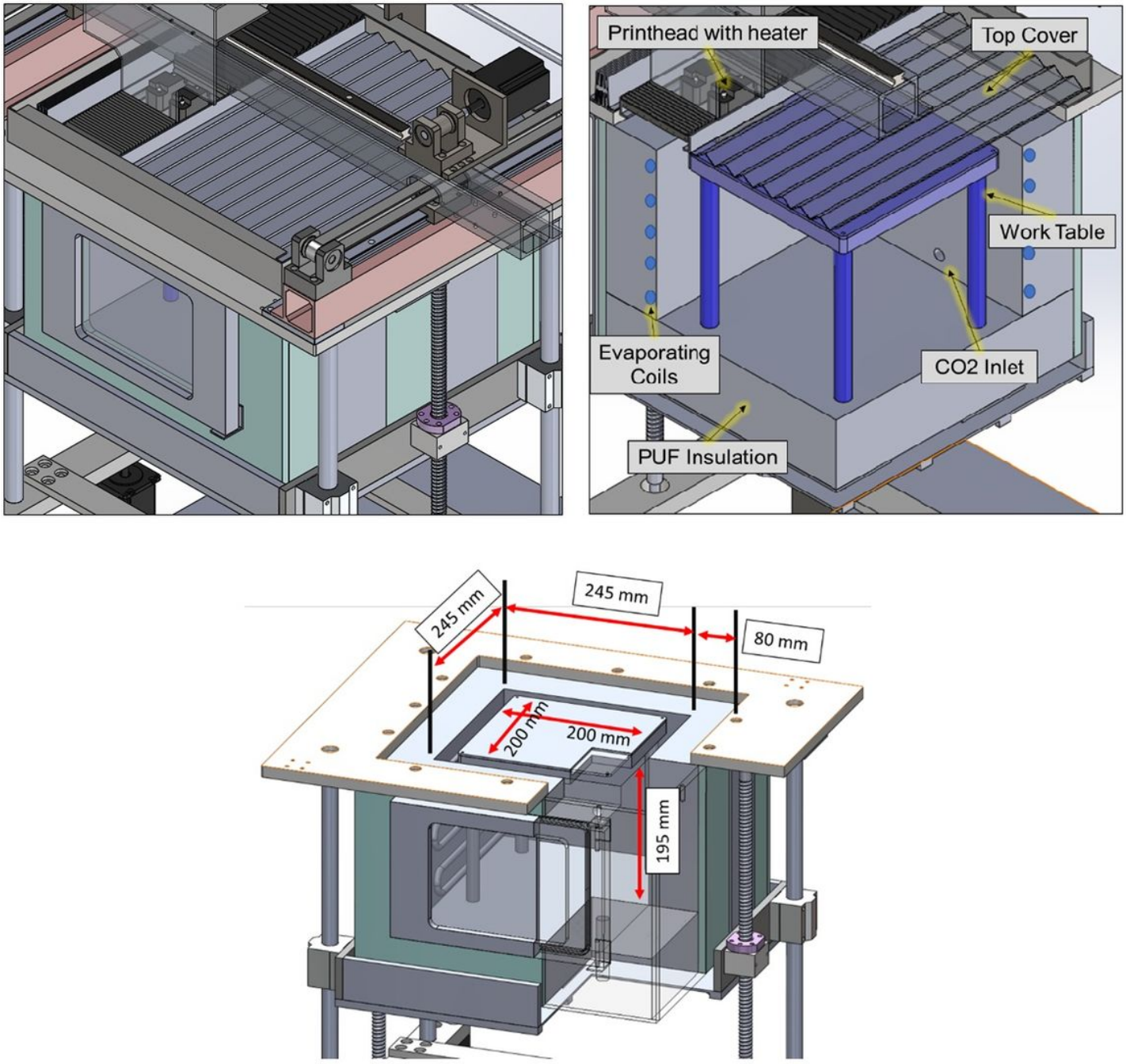

Figure 5

Architecture of the Freezing System. (a) Insulated work chamber. (b) Section view of the work chamber. (c) Dimensions of the work chamber (section view)

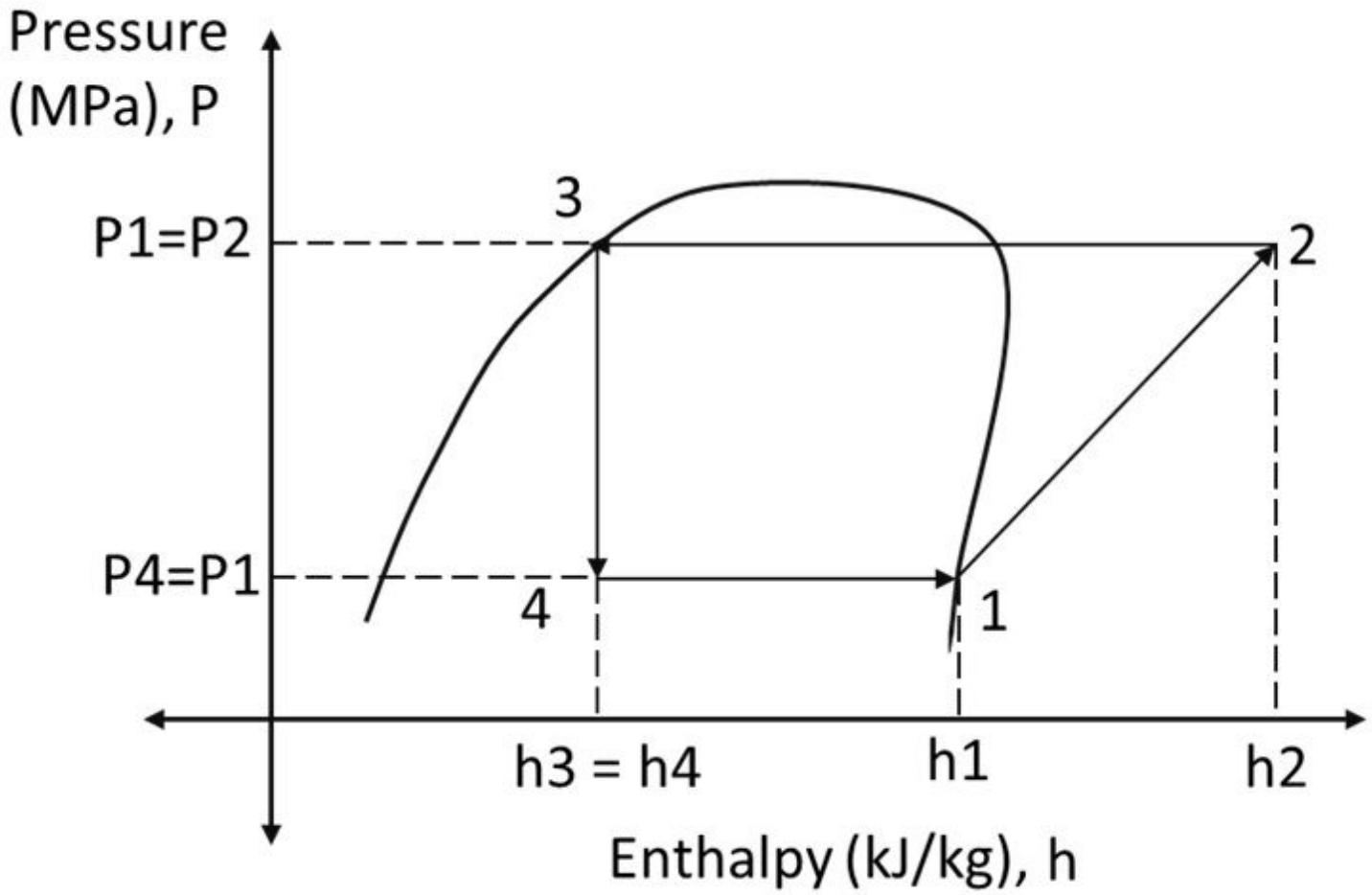

Figure 6

P-h Diagram for the Refrigerator

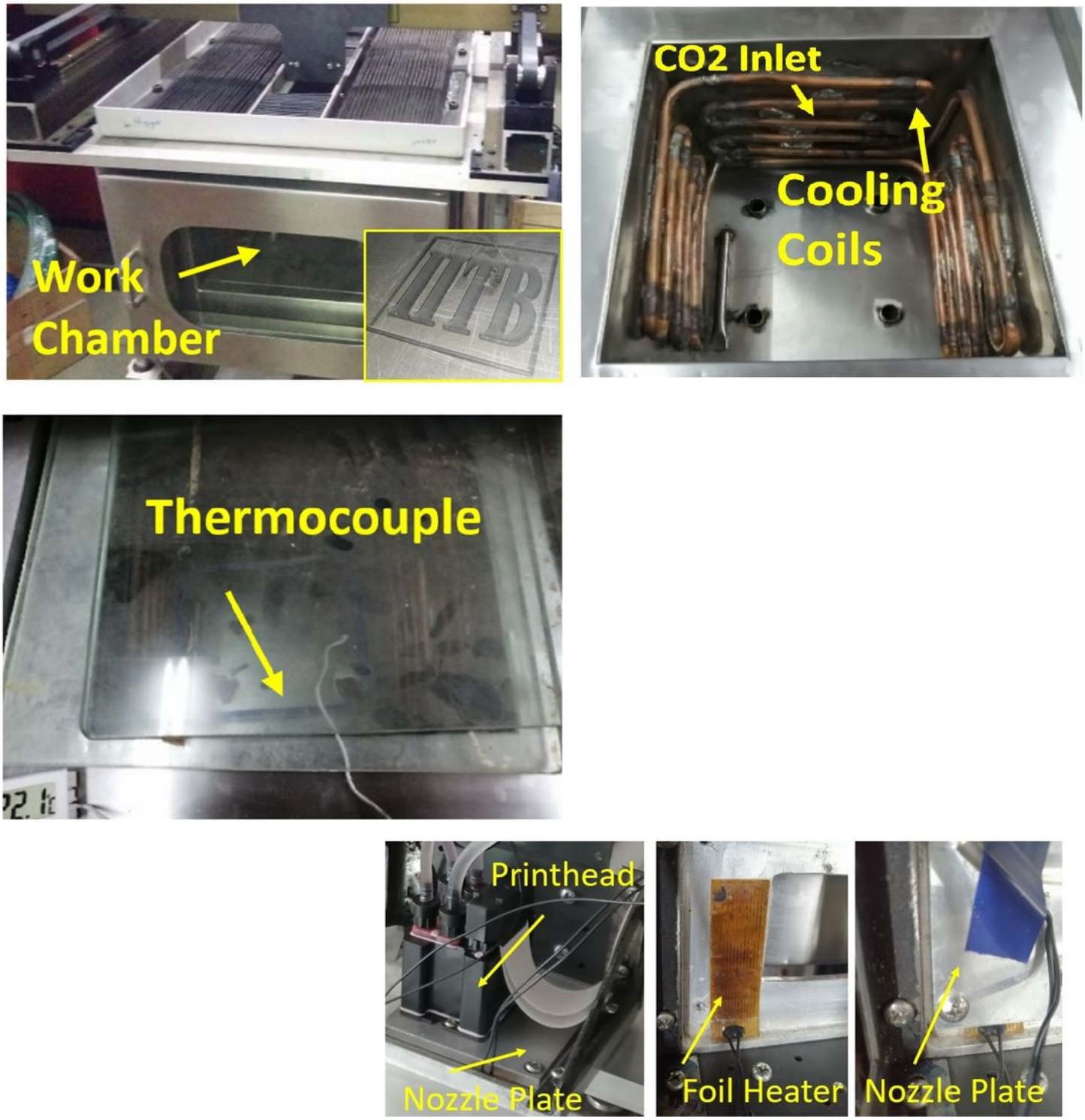

Figure 7

Experimental setup for the multimodal cooling system for ice additive manufacturing. (a) Enclosed work chamber. (b) Interior without table. (c) Thermocouple. (d) Nozzle heater arrangement.

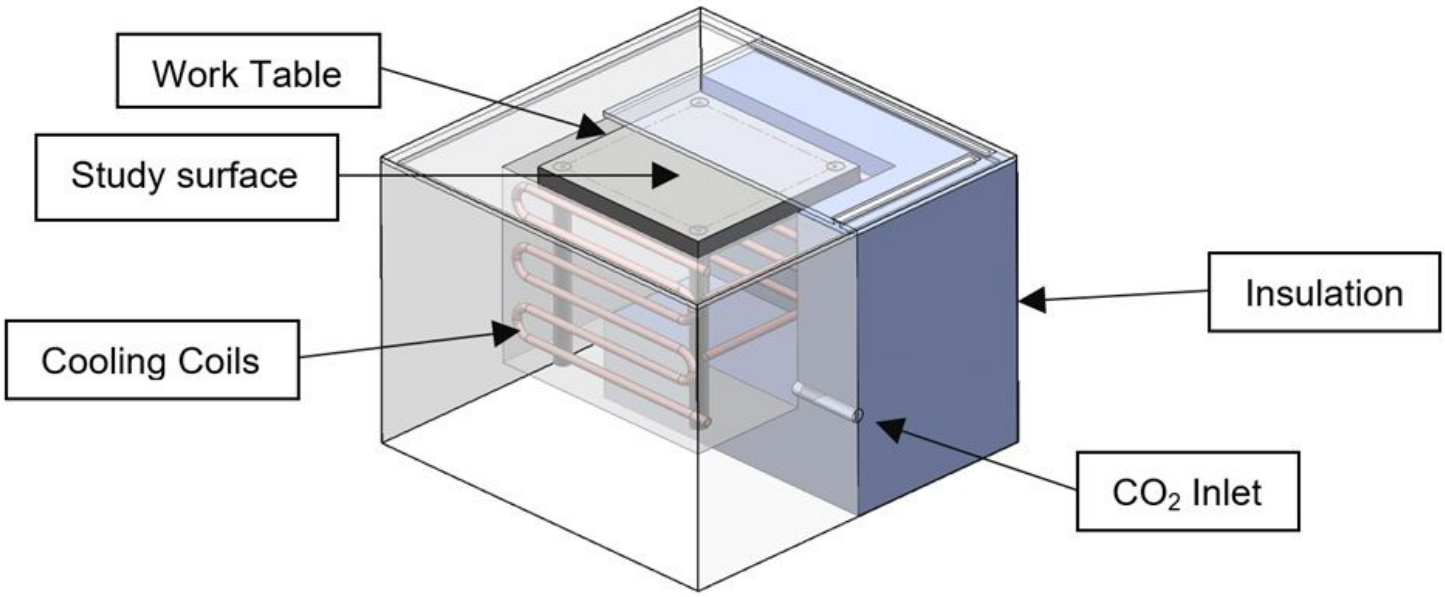

Figure 8

Section view of the geometry for the simulation

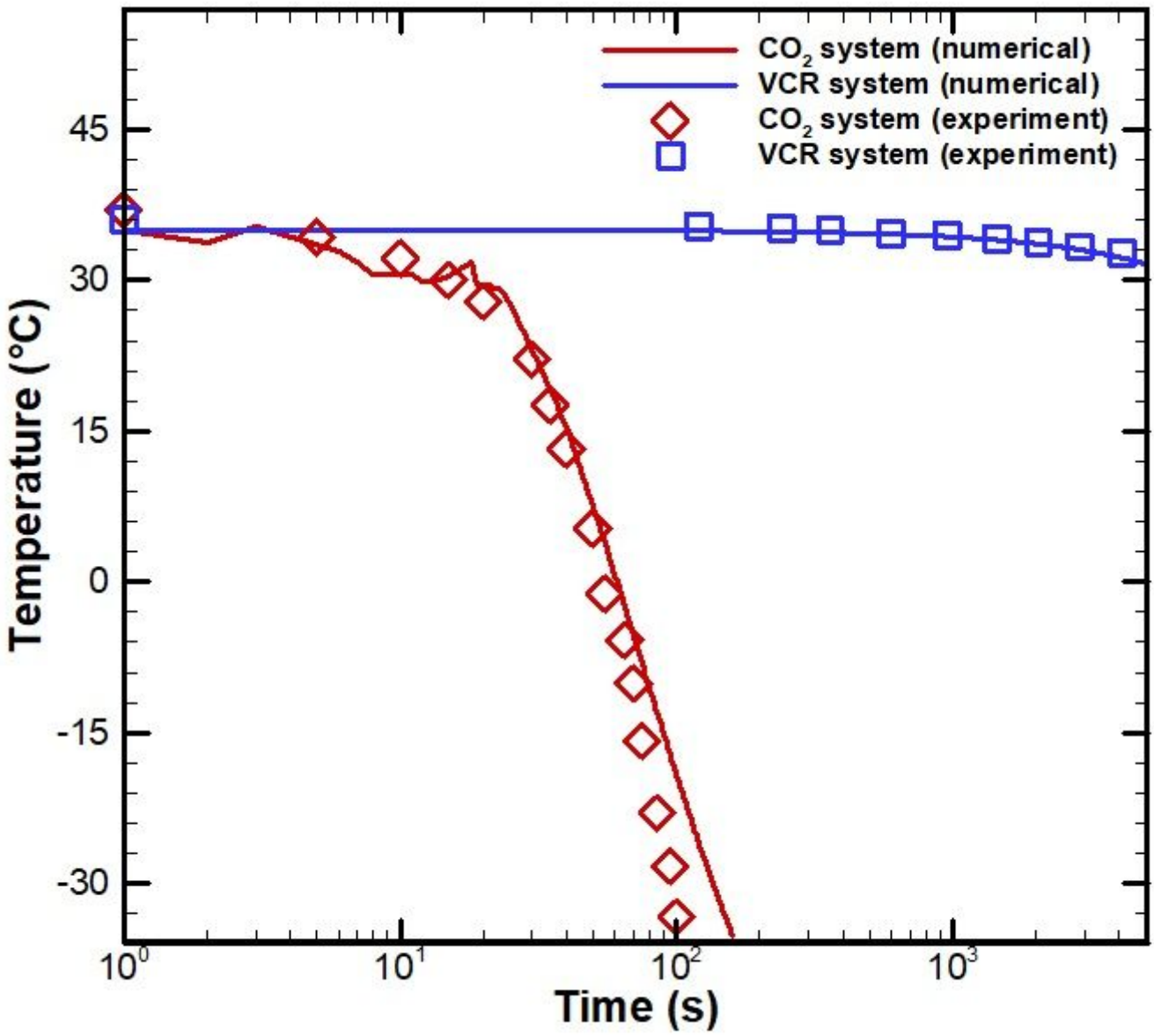

Figure 9

Time-Temperature graph for the multimodal freezing system

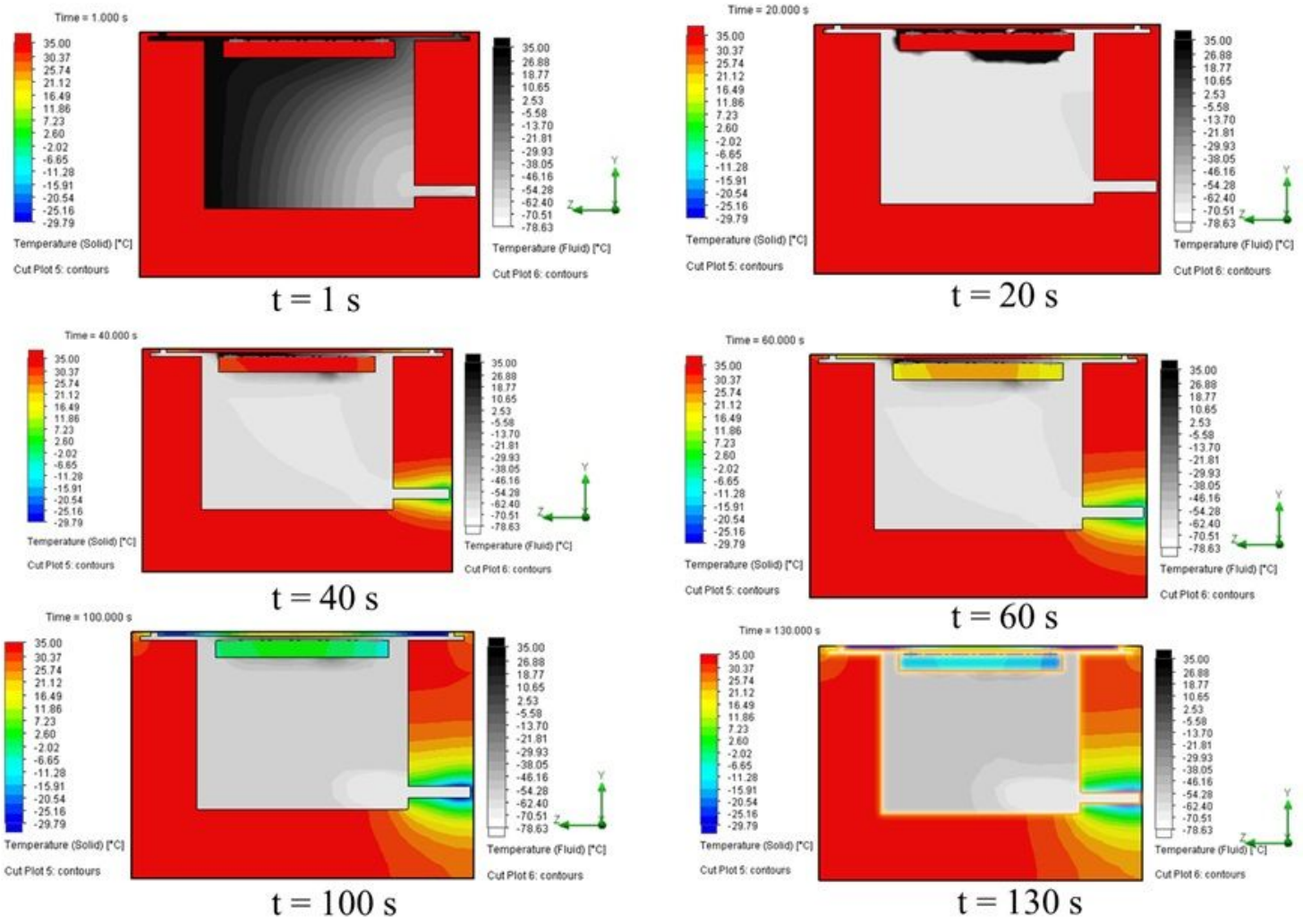

Figure 10

Temperature profile (Solid and Liquid) for CO2 system (t=125s)

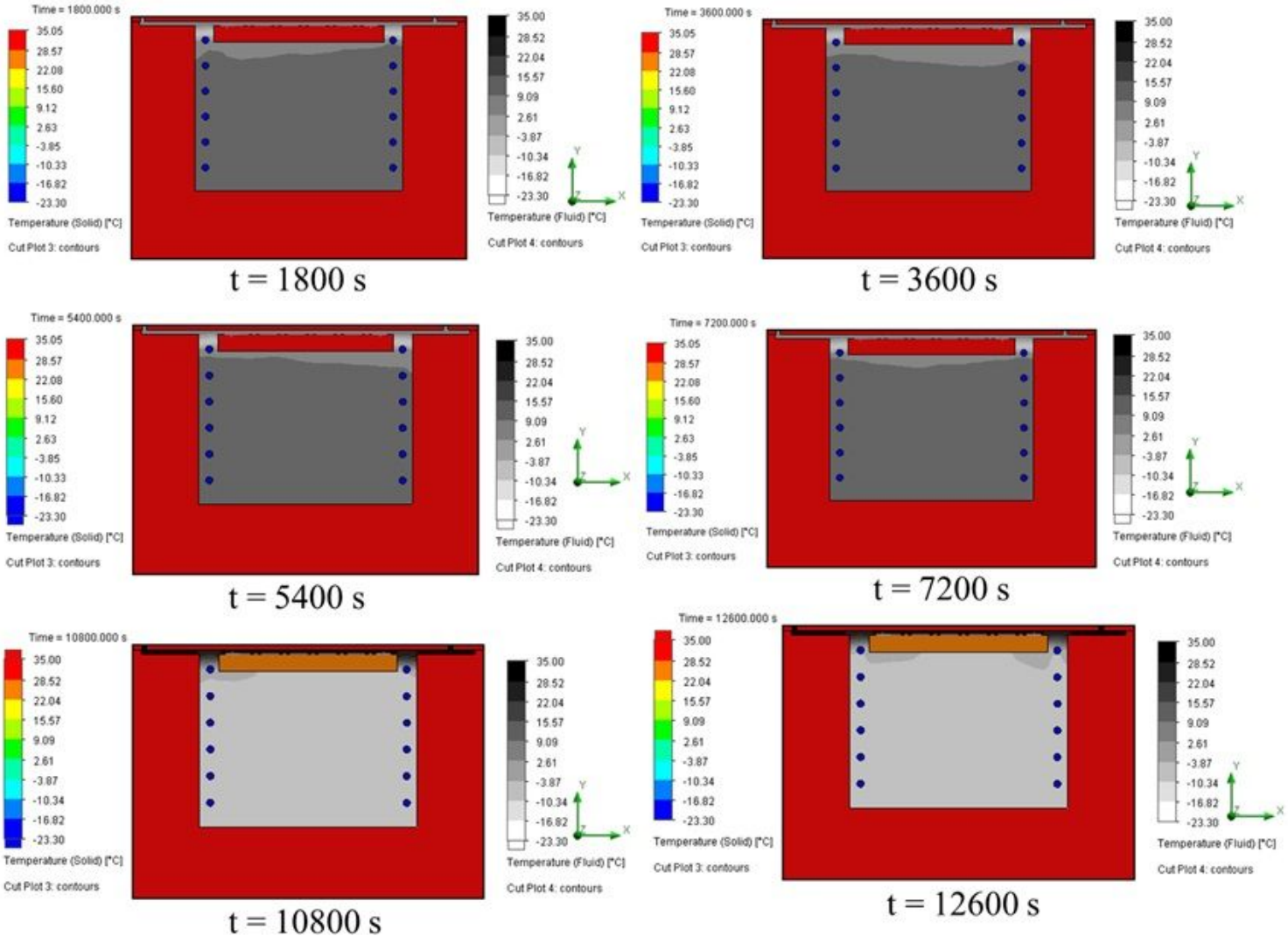

Figure 11

Temperature profile (Solid and Liquid) for VCR system (t = 15338 s)